

A Springloaded Metal-Ligand Mesocate Allows Access to Trapped Intermediates of Self-Assembly

Paul M. Bogie, Lauren R. Holloway, Yana Lyon, Nicole C. Onishi, Gregory J.O. Beran, Ryan R. Julian and Richard J. Hooley*

Department of Chemistry, University of California-Riverside, Riverside, CA 92521, United States

Supporting Information Placeholder

ABSTRACT: A strained, “springloaded” Fe₂L₃ iminopyridine mesocate shows highly variable reactivity upon post-assembly reaction with competitive diamines. The strained assembly is reactive towards transamination in minutes at ambient temperature, and allows observation of kinetically trapped intermediates in the self-assembly pathway. When diamines are used that can only form less favored cage products upon full equilibration, trapped ML₃ fragments with pendant, “hanging” NH₂ groups are selectively formed instead. Slight variations in diamine structure have large effects on the product outcome: less rigid diamines convert the mesocate to more favored self-assembled cage complexes under mild conditions and allow observation of heterocomplex intermediates in the displacement pathway. The mesocate allows control of equilibrium processes and direction of product outcomes via small, iterative changes in added subcomponent structure and provides a method of accessing metal-ligand cage structures not normally observed in multicomponent Fe-iminopyridine self-assembly.

INTRODUCTION

Reversible metal-ligand based self-assembly has enabled the creation of a variety of cage polyhedra¹ that display functions ranging from biomimetic catalysis,² to molecular recognition,³ structural switching⁴ and drug delivery.⁵ The central strategy in the self-assembly process is that the final desired product is the thermodynamic minimum: by exploiting enthalpically favorable metal-ligand coordinate bonds, the entropic penalty of bringing together multiple different components into a single assembly is overcome.⁶ As a result, the vast majority of cage assemblies are highly symmetrical: controlled formation (and characterization) of assemblies with low symmetry is less common.⁷ In addition, the vast number of moving parts in a reaction means that identifying kinetically trapped intermediates is highly challenging. There have been a number of examples of intermediate analysis in the formation of Pd-pyridyl cages,⁸ but observation of intermediates in assemblies exploiting octahedral metals is underexplored.⁹ This can be challenging due to the relatively low lability of bidentate ligands,¹⁰ which slows the dissociation rate, often requiring heating to equilibrate between different cage structures. Whereas ligand switching in Pd-pyridyl cages is quite common,¹¹ interconversion

between bidentate ligands such as catecholates and bipyridyls in cage complexes is less well known,¹² and kinetic trapping of intermediates and the formation of unfavorable cage complexes is far more difficult.

To sidestep the requirement for metal-ligand dissociation, an alternative strategy can be used. The combination of reversible, multicomponent imine formation with early transition metal salts, most usually Fe²⁺, allows access to a wide range of cage structures.¹³ The cages are usually assembled from the constituent parts by combining the metal salt, an amine and an aldehyde. If one of these components (either the amine^{14a} or the aldehyde^{14b}) is di-,¹⁵ tri-,¹⁶ or tetrapodal,¹⁷ cage polyhedra of various structures can be accessed. Transamination of the aldehyde or amine component¹⁸ is a well-known strategy for structural switching and ligand exchange in these self-assembled cages,¹⁹ and can occur rapidly, allowing facile ligand exchange in complexes that otherwise display very strong metal-ligand coordination.

However, these assemblies often require equilibration to form a single discrete product, and trapped intermediates are rarely isolated,²⁰ even though the transamination reactions can be rapid. The challenge lies in the complexity of the process: the mechanisms are far more complex

than simple metal-ligand dissociation processes, and so observing intermediates via NMR is difficult. Complexes with “hanging”, pendant amines, which are one possible intermediate in the assembly process, are not generally observed. The thermodynamic products are generally either discrete cages or coordination polymers: if the cage or macrocycle is geometrically inaccessible, polymerization is the most likely alternative rather than the formation of trapped intermediates. If the initial assembly reactions could be performed at lower temperatures, visualization of kinetically trapped intermediates is more feasible. As part of our studies on the construction and application of functionalized self-assembled cage complexes,²¹ we²² and others²³ have exploited strained, high energy assemblies to drive post-assembly ligand reactivity, additionally they can be exploited to confer social self-sorting between different ligand types.^{24,25} These assemblies can be used as starting materials for assembly of other cage structures. If the initial iminopyridine assembly is only partially stable, the transimination process will be accelerated. The challenge lies in finding a stable, yet not too stable starting assembly. Here we exploit a strained self-assembled mesocate as a “springloaded” precursor for cage assembly, and investigate its unusual reactivity patterns.

RESULTS AND DISCUSSION

The mesocate $\text{Fe}_2\text{X}_3\cdot\text{Py}_6\cdot(\text{ClO}_4)_4$ (Figure 1),^{21a} formed by heating 2,7-diaminoxanthone (**X**), 2-formylpyridine (PyCHO) and $\text{Fe}(\text{ClO}_4)_2$ in acetonitrile, is an interesting example of a strained assembly. In contrast with the many other Fe_2L_3 helicates known in the literature,²⁶ $\text{Fe}_2\text{X}_3\cdot\text{Py}_6$ is paramagnetic at room temperature and displays a red coloration indicative of a weaker ligand field than most Fe-iminopyridine complexes, which are generally diamagnetic and deep purple in color. Displacement experiments illustrate the low stability, as complete displacement of diaminoxanthone from $\text{Fe}_2\text{X}_3\cdot\text{Py}_6$ is possible upon transimination with diamines such as diamino-suberone under equilibrium conditions (70 °C, < 4 h).^{21a} We investigated its ability to act as a precursor for cage assembly by adding different aniline species to a solution of $\text{Fe}_2\text{X}_3\cdot\text{Py}_6$ in CD_3CN , and monitoring the change in NMR spectrum over time at ambient temperature. The different aniline displacer ligands used are shown in Figure 1. They range from ligands similar to diaminoxanthone **X** (diaminoxanthene **XE**, di(aminophenyl)methane **DPM** and di(aminophenyl)xanthene **DPX**), to ligands that form cages of differing stoichiometries (the diaminofluorenyl ligands **F**,^{22b} **FOH** and **FO**,⁷ and tripodal ligand **APA**²⁰).

Each ligand is based on a substituted aniline scaffold, and should displace **X** from $\text{Fe}_2\text{X}_3\cdot\text{Py}_6$ at generally similar rates. However, the reactivity profile of these ostensibly similar ligands turns out to be highly variable.

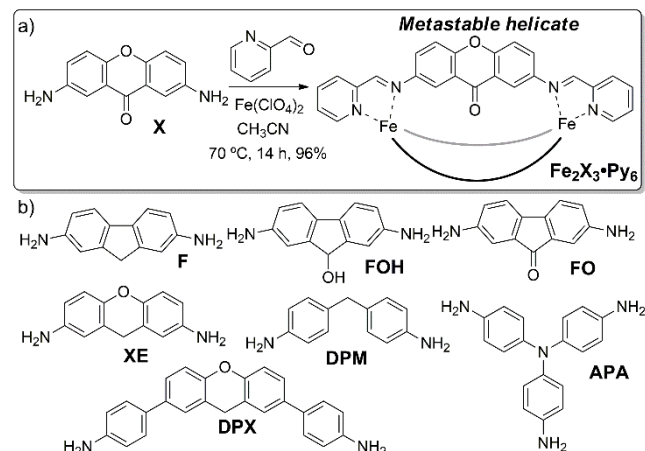


Figure 1. a) Multicomponent self-assembly of 2,7-diaminoxanthone **X** into the $\text{Fe}_2\text{X}_3\cdot\text{Py}_6$ mesocate.^{21a} b) Structures of the competitive displacer ligands used.

The initial displacement tests were performed with fluorenyl ligands **F**, **FOH** and **FO**, which are an excellent illustration of how small changes in ligand can effect large changes in cage structure. The three ligands have almost identical coordination angles, rigidities and only small variations in donor ability. **FOH**, when combined with PyCHO and $\text{Fe}(\text{ClO}_4)_2$, forms a *mer*₃*fac* M_4L_6 structure that binds one ClO_4^- ion in the cavity.⁷ In contrast, **F**, varying only by the absence of the OH group, forms an uncontrolled mixture of M_4L_6 stereoisomers.^{22b} The ketone **FO** forms a complex mixture of non-cage assemblies, presumably poorly defined aggregates and coordination polymers. All of these cages require heating to access clean, equilibrated product.

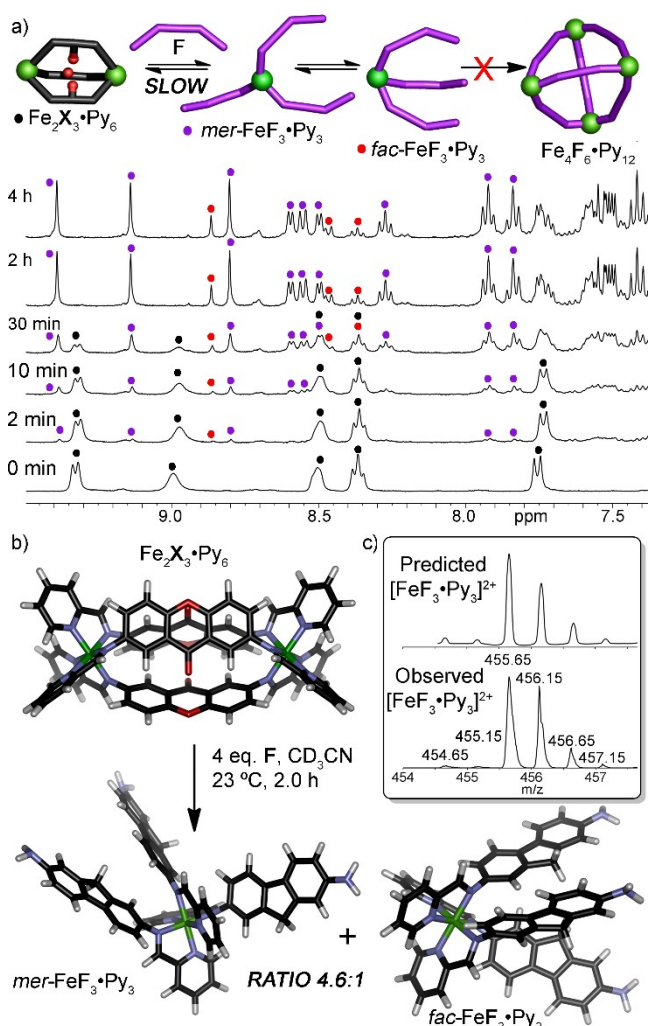


Figure 2. Deconstruction of the Fe₂X₃·Py₆ mesocate. a) Downfield regions of the ¹H NMR spectra of the addition of diaminofluorene **F** (22.9 mM) to Fe₂X₃·Py₆·(ClO₄)₄ (5.8 mM) over time (23 °C, CD₃CN, 400 MHz). b) Minimized structures of Fe₂X₃·Py₆, mer-FeF₃·Py₃ and fac-FeF₃·Py₃ (B3LYP-D3(BJ)/6-31G(d) basis set). c) Predicted vs experimentally obtained ESI-MS peaks for the [FeF₃·Py₃]²⁺ ion.

An excess (4 molar equivalents with respect to Fe₂X₃·Py₆) of diaminofluorene **F** was added to a 5.8 mM CD₃CN solution of Fe₂X₃·Py₆·(ClO₄)₄ at ambient temperature and the process monitored by NMR. As expected, the strained Fe₂X₃·Py₆ reacted rapidly, and after only 10 mins two new products were clearly visible in the ¹H NMR spectrum (Figure 2a, see Figure S-9 for full spectra). The reaction was complete after 2 h, and only Fe₂X₃·Py₆ and the two products were observable at any point in the reaction. No further reaction occurred at 23 °C, and the products were analyzed by 2D NMR and ESI-MS. No peaks corresponding to the expected Fe₄F₆·Py₁₂ cages were present. Surprisingly, the two products formed were the two isomers of the

non-cage ML₃ complex FeF₃·Py₃, along with excess ligand **F** and expunged **X**. The complexity of the NMR stems from the fact that the *mer* isomer does not have C₃ symmetry, and so all peaks from the fluorenyl ligand are tripled in the NMR spectrum.²⁷ The *fac:mer* ratio was 1:4.6, and this ratio (within integration error) was consistent throughout the reaction. 2D COSY and DOSY NMR experiments clearly showed the presence of the two isomers, and ESI-MS analysis corroborates the assignment. No heterocomplexes were observed, only peaks for [FeF₃·Py₃]²⁺ and a [FeF₂·Py₂]²⁺ fragment, plus small peaks from the Fe₂X₃·Py₆ reactant and ligands **F** and **X** (Figure 2c, see Figure S-40 for full spectrum). In addition, an ML₃ complex, independently synthesized from p-phenetidine, Fe(ClO₄)₂ and PyCHO, displayed NMR spectra that were consistent with the *fac:mer* mixture seen with FeF₃·Py₃ (see Figure S-33), although with a higher proportion of *mer* isomer present (*fac:mer* ratio = 1:10.7).

Despite the general favorability of cage assembly in these systems, the presence of reactive diaminofluorene **X**, the “hanging” amine groups in FeF₃·Py₃ and the fact that Fe₂X₃·Py₆ is *thermodynamically favored* over a combination of **X**, Fe²⁺ and PyCHO, the ML₃ fragment is completely favored in this system. In addition, no evidence of any incorporation of diaminofluorene **X** in the final product was observed, only homocomplex FeF₃·Py₃. This was surprising, as we are aware of only one self-assembled system that is tolerant to free NH₂ groups; that of the assembly of tripodal ligands such as **APA** (vide infra).²⁰ In our hands,^{7,21,22} all types of Fe₂L₃ or Fe₄L₆ cages react with diamines in one of three ways: complete displacement by the incoming ligand (leading to Fe_xL₂_y + amine **L1**), no reaction (leading to Fe_xL₁_y + amine **L2**), or partial displacement leading to heterocomplexes and/or decomposition. Despite this, the FeF₃·Py₃ mixture was stable: no conversion to other products was seen at 23 °C for multiple days, and the product could be cleanly isolated from the reaction mixture by precipitation and washing. No conversion to the Fe₄F₆·Py₁₂ cage was seen upon heating to 70 °C for 16 h, and more extensive heating led only to decomposition. In attempt to determine whether FeF₃·Py₃ is an intermediate on the path to Fe₄F₆·Py₁₂, diaminofluorene **F**, Fe(ClO₄)₂ and PyCHO were reacted for 2 h in CD₃CN at 23 °C, conditions that are too mild to effect cage formation (see Figure S-35). In this case, no peaks for either the *fac* or *mer* ML₃ fragment were observed, only a complex mixture of products and starting materials. However, upon heating, Fe₄F₆·Py₁₂ was formed as expected.

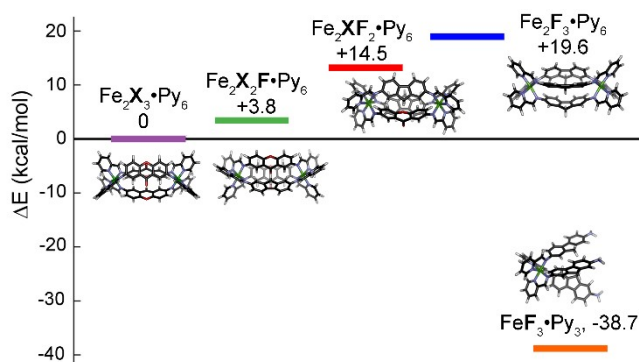


Figure 3. Relative single point energies (B3LYP-D3(BJ)/def2-TZVP in implicit acetonitrile) of mixed **X/F** Fe_2L_3 heterocomplexes, reactant $\text{Fe}_2\text{X}_3\cdot\text{Py}_6$ and product $\text{fac-FeF}_3\cdot\text{Py}_3$ in kcal/mol.

Evidently the xanthone starting material forces the reaction to an outcome unobserved with the simple amine/aldehyde assembly process. The unfavorability of both the reactant $\text{Fe}_2\text{X}_3\cdot\text{Py}_6$ and the putative cage product $\text{Fe}_4\text{F}_6\cdot\text{Py}_{12}$ cause the system to form the only favorable possibility left, $\text{FeF}_3\cdot\text{Py}_3$. Dispersion-corrected density functional theory calculations were performed to shed light on this (Figure 3), and it was immediately obvious that the mixed mesocate heterocomplexes are extremely strained and even more disfavored than $\text{Fe}_2\text{X}_3\cdot\text{Py}_6$. The geometries of the possible M_2L_3 heterocomplexes ($\text{Fe}_2\text{X}_2\text{F}\cdot\text{Py}_6$, $\text{Fe}_2\text{XF}_2\cdot\text{Py}_6$, $\text{Fe}_2\text{F}_3\cdot\text{Py}_6$) were optimized using B3LYP-D3(BJ) in the 6-31G(d) basis set and implicit acetonitrile polarizable continuum solvent, followed by single point energy refinement in the larger def2-TZVP basis set.²⁸ These energies were then compared to those of $\text{Fe}_2\text{X}_3\cdot\text{Py}_6$ and two equivalents of $\text{fac-FeF}_3\cdot\text{Py}_3$. The sequential replacement of each **X** ligand in the M_2L_3 mesocate structure by an **F** ligand causes an increase in energy, with $\text{Fe}_2\text{F}_3\cdot\text{Py}_6$ being 19.6 kcal mol⁻¹ less stable than $\text{Fe}_2\text{X}_3\cdot\text{Py}_6$. In contrast, the opened $\text{fac-FeF}_3\cdot\text{Py}_3$ product is over 38 kcal/mol more stable than $\text{Fe}_2\text{X}_3\cdot\text{Py}_6$. The concept of a “goldilocks” scheme²⁴ is present here: neither reactant $\text{Fe}_2\text{X}_3\cdot\text{Py}_6$ or putative product $\text{Fe}_4\text{F}_6\cdot\text{Py}_{12}$ are particularly favorable assemblies, and so the system forms the only other stable product outcome, $\text{FeF}_3\cdot\text{Py}_3$, despite the presence of hanging, reactive NH_2 groups.

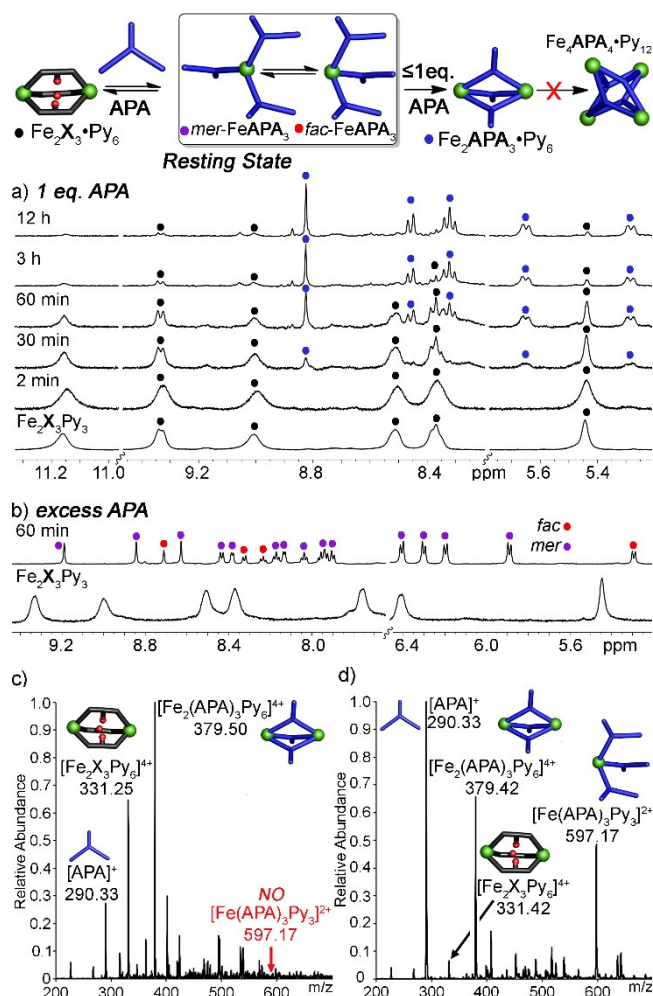


Figure 4. Concentration-dependent Reactivity. a,b) Downfield regions of the ^1H NMR spectra of the addition of varying concentrations of **APA** (a = 14.2 mM, b = 22.5 mM) to $\text{Fe}_2\text{X}_3\cdot\text{Py}_6\cdot(\text{ClO}_4)_4$ (5.8 mM) over time (23 °C, CD_3CN , 400 MHz). c) ESI-MS spectrum of the reaction mixture from a) after 45 min reaction time. d) ESI-MS spectrum of the reaction mixture from b) after 45 min reaction time.

Addition of the two other fluorenyl variants **FOH** and **FO** to $\text{Fe}_2\text{X}_3\cdot\text{Py}_6$ in CD_3CN gave even more surprising results. Diaminofluoreneol **FOH** forms a very stable M_4L_6 structure in the presence of ClO_4^- ions,⁷ but when added to $\text{Fe}_2\text{X}_3\cdot\text{Py}_6$, a mixture of products was formed, with no peaks that corresponded to $\text{Fe}_4\text{FOH}_6\cdot\text{Py}_{12}$ or the $\text{FeFOH}_3\cdot\text{Py}_3$ complex. Diaminofluorenone **FO** showed no reactivity at all. When an excess was added to a solution of $\text{Fe}_2\text{X}_3\cdot\text{Py}_6$ in CD_3CN , the peaks for **FO** were broad and ill-defined, but the meta-stable $\text{Fe}_2\text{X}_3\cdot\text{Py}_6$ was unchanged, even after 2 days reaction. More extensive heating to drive the reaction to product caused decomposition. Despite the similarity in nucleophilicity between **F**, **FOH** and **FO**, only **F** was able to form a discrete product when added to $\text{Fe}_2\text{X}_3\cdot\text{Py}_6$.

To see if these variations in reactivity were a general phenomenon, we analyzed a ligand that is known to tolerate hanging amine groups in its assembly: tripodal ligand **APA**. This ligand has been shown by the Nitschke group to form either the kinetically trapped M_{2L_3} mesocate $Fe_2\mathbf{APA}_3\cdot Py_6$ with three unreacted NH_2 groups present, or the fully reacted M_{4L_4} tetrahedral cage $Fe_4\mathbf{APA}_4\cdot Py_{12}$ when APA is reacted with Fe^{2+} salts and PyCHO.²⁰ The product outcome depends on the proportions of PyCHO/ Fe^{2+} and temperature: mesocate $Fe_2\mathbf{APA}_3\cdot Py_6$ can be converted to cage $Fe_4\mathbf{APA}_4\cdot Py_{12}$ upon heating. The mesocate can form at 23 °C, whereas the M_{4L_4} requires heating at 80 °C for 11 days to effect full equilibration.

Using the same procedure as for **F**, **APA** was added to a solution of $Fe_2\mathbf{X}_3\cdot Py_6$ in CD_3CN and the reaction monitored by NMR (Figure 4a). Initially, only a single equivalent of **APA** (with respect to **X** in $Fe_2\mathbf{X}_3\cdot Py_6$) was used (see Figure S-22 for full spectra). Only one product was observed in this case, mesocate $Fe_2\mathbf{APA}_3\cdot Py_6$. No M_{4L_4} cage or ML_3 fragments were observed at any time. However, when $Fe_2\mathbf{X}_3\cdot Py_6$ was subjected to an excess of **APA** (up to 4 eq. with respect to **X** in $Fe_2\mathbf{X}_3\cdot Py_6$), no $Fe_2\mathbf{APA}_3\cdot Py_6$ mesocate was seen (see Figure 4b and Figure S-23). Instead, the two isomers of the ML_3 fragment $Fe\mathbf{APA}_3\cdot Py_3$ formed, with a *fac:mer* ratio was almost identical to that of $Fe\mathbf{F}_3\cdot Py_3$ at 1:4.3. The ML_3 mixture was not completely stable: the product could be isolated in sufficient purity for NMR analysis, but decomposed within 24 h. If the $Fe\mathbf{APA}_3\cdot Py_3$ mixture was heated to 70 °C for 2 h, complete conversion to $Fe_2\mathbf{APA}_3\cdot Py_6$ was observed. Interestingly, we were unable to access the M_{4L_4} tetrahedron using this method. More extensive heating caused decomposition, and no evidence of $Fe_4\mathbf{APA}_4\cdot Py_{12}$ could be seen. This is not too surprising, as the proportions of Fe to PyCHO are fixed at a 2:3 ratio by the $Fe_2\mathbf{X}_3\cdot Py_6$ reactant (an incorrect stoichiometry for M_{4L_4} formation), but it is another example of biased reactivity. When formed from the aldehyde and amine, $Fe_2\mathbf{APA}_3\cdot Py_6$ can easily be converted to $Fe_4\mathbf{APA}_4\cdot Py_{12}$ upon further heating the reaction mixture. As there is minimal aldehyde present in our case, this interconversion is prevented.

The **APA** and **F** ligands illustrate the strained nature of $Fe_2\mathbf{X}_3\cdot Py_6$. Upon addition of competitive ligand, reversible transimination occurs, springing open the strained $Fe_2\mathbf{X}_3\cdot Py_6$ mesocate. The initial product formed in each case is the opened ML_3 complex, but the reaction outcomes vary from there. In the case of **F**, no further reaction is observed, as there are no other viable assemblies to access. In the case of **APA**, the ML_3 mixtures are only transient intermediates. If

[**APA**] is low, steady state kinetics are observed, and no intermediates are seen during the slow equilibration to $Fe_2\mathbf{APA}_3\cdot Py_6$. If [**APA**] is high, the equilibrium is biased towards the ML_3 complex, and the result is a resting state of $Fe\mathbf{APA}_3\cdot Py_3$. This is a kinetic resting state, however, and can be easily driven to the thermodynamically favored M_{2L_3} product upon mild heating. The reaction outcomes are controlled by the product structure: the ML_3 complexes are not affected by strain, coordination angle or other supramolecular effects, but their formation lies in the (lack of) stability of the other possible products.

We next investigated ligands that are very similar in structure to **X**. Diaminoxanthene **XE** and di(aminophenyl)xanthene **DPX** are different from **X** in only two ways: greater electron donor ability (in both cases) and length (in the case of **DPX**). We have previously shown that diaminoxanthene forms a stable M_{2L_3} mesocate upon self-assembly with $Fe(ClO_4)_2$ and PyCHO.^{22b} Diaminoxanthene **XE** was added to a solution of $Fe_2\mathbf{X}_3\cdot Py_6$ in CD_3CN and the reaction monitored at 23 °C by NMR (see Figures 5a and S-29). After < 2 mins reaction, no peaks for $Fe_2\mathbf{X}_3\cdot Py_6$ remained in the ¹H NMR spectrum, only a single new product (plus residual diamines **X** and **XE**). The peaks for the new product did not match those of the expected $Fe_2\mathbf{XE}_3\cdot Py_6$ mesocate, however. The initial product formed was the opened ML_3 complex $Fe\mathbf{XE}_3\cdot Py_3$, but in this case, only a single *fac* isomer was formed. The product is symmetrical, and the ¹H NMR peaks in the iminopyridine region match those of the other two observed *fac* ML_3 species, $Fe\mathbf{F}_3\cdot Py_3$ and $Fe\mathbf{APA}_3\cdot Py_3$. In contrast to those ML_3 fragments, however, the xanthene equivalent was only observed transiently. Over time, new peaks grew in to the NMR spectrum, corresponding exactly to those of the self-assembled $Fe_2\mathbf{XE}_3\cdot Py_6$ mesocate. After 24 h, ~50 % conversion is seen, and complete reaction requires 16 h heating at 70 °C. The reaction is clean, and no other intermediates are observed: the diaminoxanthene **XE** rapidly displaces the xanthene **X**, followed by a slow equilibration to the final $Fe_2\mathbf{XE}_3\cdot Py_6$ mesocate.

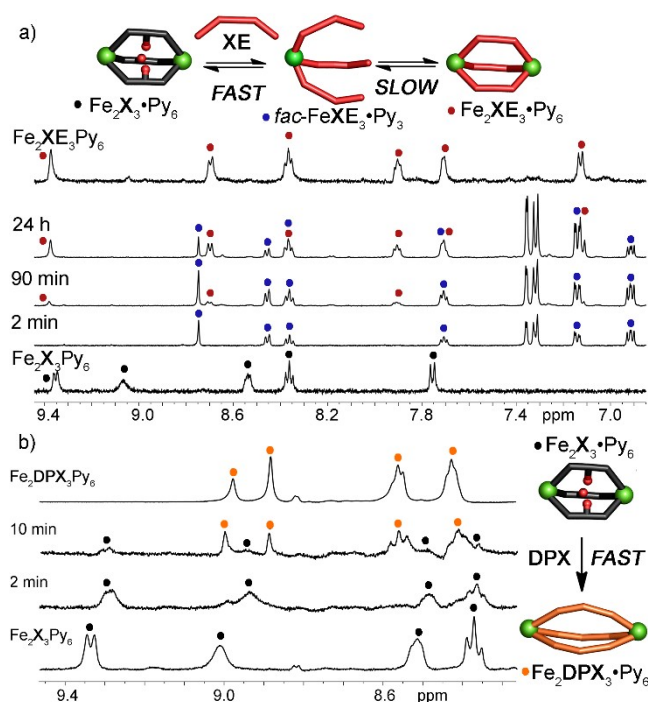


Figure 5. Length-dependent reactivity. a) Downfield regions of the ^1H NMR spectra of the addition of diaminoxanthene **XE** (17.7 mM) to $\text{Fe}_2\text{X}_3\cdot\text{Py}_6\cdot(\text{ClO}_4)_4$ (5.8 mM) over time. (23 $^\circ\text{C}$, CD_3CN , 400 MHz). b) Downfield regions of the ^1H NMR spectra of the addition of extended xanthyl ligand **DPX** (17.6 mM) to $\text{Fe}_2\text{X}_3\cdot\text{Py}_6\cdot(\text{ClO}_4)_4$ (5.8 mM) over time.

The extended di(aminophenyl)xanthene **DPX** shows different behavior again (see Figures 5b and S-31). In this case, the reaction is also extremely rapid, and is complete in < 10 mins. The products are a mixture of the helicate and mesocate isomers of the $\text{Fe}_2\text{DPX}_3\cdot\text{Py}_6$ assembly, presumably due to the greater flexibility in the extended **DPX** ligand.^{15,21d} The same product outcome is formed when **DPX** is combined with $\text{Fe}(\text{ClO}_4)_2$ and PyCHO (for full characterization, see Supporting Information). The reaction is so rapid that no fragments or intermediates could be observed, and if the ML_3 fragment is formed in this case, it is significantly less favorable than the helicate products. Despite the fact that **DPX** is slightly less nucleophilic than **XE**, the transimination reaction is significantly faster than with **XE**. In both cases, the initial disruption of the $\text{Fe}_2\text{X}_3\cdot\text{Py}_6$ assembly is rapid, but the conversion of $\text{FeXE}_3\cdot\text{Py}_3$ to $\text{Fe}_2\text{XE}_3\cdot\text{Py}_6$ is slow. Although no $\text{FeDPX}_3\cdot\text{Py}_3$ can be observed, it is reasonable to assume that the reaction goes *via* that intermediate, but the second step is fast in this case, and steady state kinetics are active, so only $\text{Fe}_2\text{DPX}_3\cdot\text{Py}_6$ is observed.

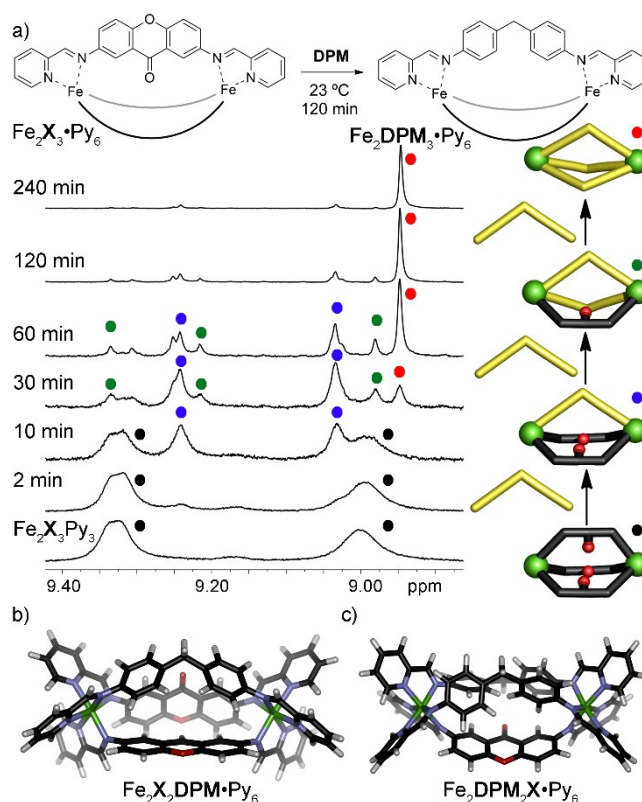


Figure 6. Transient Heterocomplex Formation. a) Downfield regions of the ^1H NMR spectra of the addition of diaminodiphenylmethane **DPM** (36.7 mM) to $\text{Fe}_2\text{X}_3\cdot\text{Py}_6\cdot(\text{ClO}_4)_4$ (5.8 mM) over time. (23 $^\circ\text{C}$, CD_3CN , 400 MHz). b) Minimized structures of heterocomplexes b) $\text{Fe}_2\text{X}_2\text{DPM}\cdot\text{Py}_6$, c) $\text{Fe}_2\text{DPM}_2\text{X}\cdot\text{Py}_6$ (B3LYP-D3(BJ)/6-31G(d) basis set).

Finally, we tested the simplest diamine displacer ligand, di(aminophenyl)methane **DPM**, which forms a highly stable M_2L_3 mesocate; the Ru equivalent is sufficiently stable *in vivo* to be an effective anti-cancer agent.²⁹ The mesocate forms in < 2 h at 23 $^\circ\text{C}$ from **DPM**, $\text{Fe}(\text{ClO}_4)_2$ and PyCHO , so equilibration to the thermodynamic product is rapid. **DPM** is flexible, so is capable of rotating to achieve various coordination angles upon assembly. Interestingly, when **DPM** was added to a $\text{Fe}_2\text{X}_3\cdot\text{Py}_6$ solution, no evidence of ML_3 fragments was seen: instead, $\text{Fe}_2\text{X}_3\cdot\text{Py}_6$ was converted to $\text{Fe}_2\text{DPM}_3\cdot\text{Py}_6$ *via* a series of M_2L_3 heterocomplexes, as shown in Figure 6. The displacement occurs rapidly: after only 10 mins, peaks for the $\text{Fe}_2\text{X}_2\text{DPM}\cdot\text{Py}_6$ heterocomplex are seen. For clarity, only the imine CH region is shown in Figure 6 (see S-32 for full spectra). After 30 mins, the peaks for $\text{Fe}_2\text{X}_2\text{DPM}\cdot\text{Py}_6$ recede and new peaks for $\text{Fe}_2\text{X}\cdot\text{DPM}_2\cdot\text{Py}_6$ grow in, followed by those for $\text{Fe}_2\text{DPM}_3\cdot\text{Py}_6$ product. After 2 h, the reaction is complete, and only the equilibrated mesocate is observed. In this case, the reaction is not controlled by opening the strained $\text{Fe}_2\text{X}_3\cdot\text{Py}_6$, but by the stability of the product

helicate $\text{Fe}_2\text{DPM}_3\cdot\text{Py}_6$. The **DPM** ligand has the same length as diaminoxanthone **X**, and its additional flexibility allows incorporation into heterocomplex assemblies, which are more stable than the opened ML_3 fragments. The stability of the $\text{Fe}_2\text{DPM}_3\cdot\text{Py}_6$ product allows this ligand to behave as expected: only iminopyridine products are seen, with no “hanging” NH_2 groups. As there is a stable cage outlet for the transimination reaction, the process is directed to that product.

A schematic summary of the reaction outcomes is shown in Figure 7. The seven aniline components used here vary only slightly in nucleophilicity, yet the reaction time for displacement of **X** from $\text{Fe}_2\text{X}_3\cdot\text{Py}_6$ varies from < 2 mins (**DPX**) to multiple hours (**F**) and in one case, no reaction occurs at all (**FO**). The product outcomes are different: in cases where the product cage is disfavored (e.g. **F**), stable FeL_3 complexes containing “hanging” NH_2 groups form. These ML_3 complexes can vary in their isomeric ratio: *mer* is generally favored over *fac*, except in the case of addition of **XE**, where only the *fac* isomer is formed, and then only transiently. This *fac*- $\text{FeXE}_3\cdot\text{Py}_3$ complex is formed almost instantaneously, yet slowly closes to the $\text{Fe}_2\text{XE}_3\cdot\text{Py}_6$ mesocate upon standing. The extended **DPX** component shows no intermediates or fragments and forms the favored $\text{Fe}_2\text{DPX}_3\cdot\text{Py}_6$ mesocate very rapidly. Addition of **DPM** also gives the favored $\text{Fe}_2\text{DPM}_3\cdot\text{Py}_6$ mesocate, but in this case, the individual heterocomplexes can be transiently observed during the reaction.

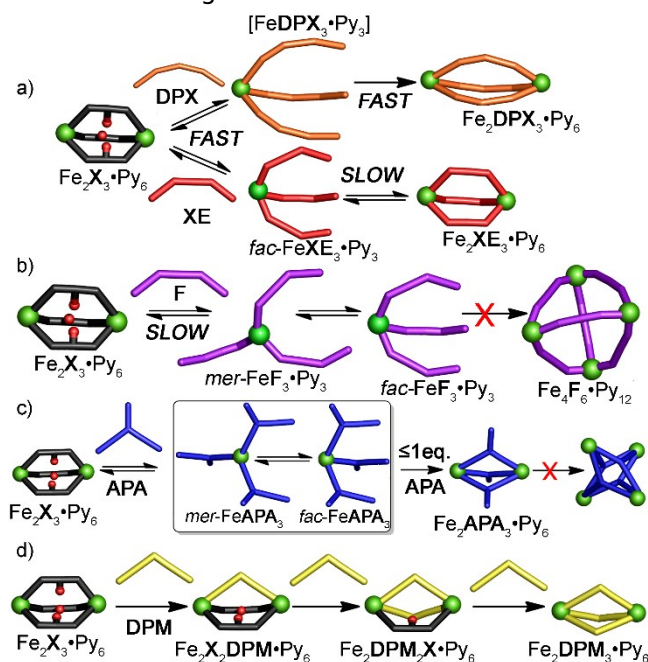


Figure 7. Summary of reaction outcomes upon addition of competitive amine ligands to $\text{Fe}_2\text{X}_3\cdot\text{Py}_6$.

a) Xanthenyl ligands **XE**, **DPX**; b) Fluorene **F**; c) tripodal ligand **APA**; d) flexible ligand **DPM**.

The $\text{Fe}_2\text{X}_3\cdot\text{Py}_6$ mesocate is unique: it is sufficiently stable to be formed *via* self-assembly with PyCHO , **X** and Fe^{2+} salts, yet unstable enough to be displaced by added di- (or)-tri-aniline at room temperature. Furthermore, the reaction outcomes are highly variable, and often controlled by the nature of the incoming subcomponent. These highly disparate reactivity patterns are extremely unusual, but some mechanistic conclusions can be drawn. The initial addition of diamine to $\text{Fe}_2\text{X}_3\cdot\text{Py}_6$ is reversible and fast, potentially occurring in seconds at ambient temperature. The speed of the initial reaction indicates that transimination is the prevalent mechanism, not a dissociation of the iminopyridine arm from the Fe^{2+} center, driven by the Lewis acidic Fe^{2+} ions and the strain release upon opening of the $\text{Fe}_2\text{X}_3\cdot\text{Py}_6$ mesocate. After initial addition, the outcome is controlled by the favorability (or lack thereof) of the products. If the final product assembly has a high barrier to equilibration ($\text{Fe}_4\text{F}_6\cdot\text{Py}_{12}$ or $\text{Fe}_4\text{APA}_4\cdot\text{Py}_{12}$), then an equilibrating *fac/mer* mixture of FeL_3 fragments with pendant amines is the default product. Heating these fragments allows equilibration to the thermodynamic product in some cases, although the presence of multiple diamine species in solution can interrupt this process (especially for **FOH**). If the target cage assembly is favorable, the equilibration to product is observed, at a rate dependent on the stability of the assembly. In these cases (with diamines **XE** or **DPX**), the $\text{Fe}_2\text{X}_3\cdot\text{Py}_6$ precursor is rapidly broken open, then “snaps shut”. Finally, in the case of more flexible diamines such as **DPM**, sufficient strain release is possible upon displacing diaminoxanthone from $\text{Fe}_2\text{X}_3\cdot\text{Py}_6$ that the conversion to thermodynamic mesocate $\text{Fe}_2\text{X}_3\cdot\text{Py}_6$ occurs via iterative formation of $\text{Fe}_2\text{L}^1\text{L}^2$ mesocates. The mild conditions allow observation of these heterocomplexes as transient intermediates in that case, something very rarely seen in multicomponent self-assembly.

Still, some questions remain unanswered. It is not at all clear why addition of diaminoxanthone **XE** to $\text{Fe}_2\text{X}_3\cdot\text{Py}_6$ leads to formation of only the *fac* isomer of the ML_3 fragment (followed by slow collapse to the M_2L_3 product), whereas all other cases give a mixture favoring the *mer* isomer. The complete exclusion of diaminoxanthone **X** from the ML_3 fragments is also unusual: there are no strain considerations in the non-cage ML_3 fragments, so the complete preference for FeF_3 in the presence of **X** is highly surprising. The formation of self-assembled cages and helicates is a delicate combination of donor ability and

coordination geometry, and accurate determination of all the possible factors controlling reactivity is challenging. Still, the $\text{Fe}_2\text{X}_3\cdot\text{Py}_6$ mesocate provides a unique insight into the mechanism for formation of Fe-iminopyridine cages, and allows redirection of product outcomes from the usual suspects.

CONCLUSIONS

Employing a strained Fe-iminopyridine mesocate assembly as a reactant for self-assembled cage synthesis instead of the usual metal salt/aldehyde/polyamine strategy allows observation of unusual reaction outcomes. Whereas most known cage complexes are the thermodynamically favored product, and are accessed via equilibration conditions, the springloaded nature of the $\text{Fe}_2\text{X}_3\cdot\text{Py}_6$ mesocate allows reaction and formation of discrete, observable intermediates under mild, kinetically controlled conditions. The cage shows highly variable reactivity upon treatment with competitive diamines. Kinetically trapped ML_3 fragments with pendant, "hanging" NH_2 groups are selectively formed over less favorable cage complexes. When amines that allow more favored cage assemblies are used, ML_3 fragments are either observed as intermediates or bypassed entirely on route to highly favored complexes. Flexible diamines convert the assembly to more favored self-assembled cage complexes under mild conditions via heterocomplex $\text{Fe}_2\text{L}^1\text{xL}^2\text{y}$ mesocate intermediates in the displacement pathway. The strained nature of the mesocate provides the impetus for the reaction, and the final outcome is determined by the product stability. The use of strained precursors allows redirection of normal reactivity patterns, and may well provide a useful method for the construction of more non-symmetrical, complex cage structures, a strategy we are currently investigating.

EXPERIMENTAL SECTION

General Information

^1H and ^{13}C spectra were recorded on a Bruker Avance NEO 400 NMR spectrometer. 2D NMR spectra were obtained on a Bruker Avance 600 MHz NMR spectrometer. Proton (^1H) chemical shifts are reported in parts per million (δ) with respect to tetramethylsilane (TMS, $\delta=0$), and referenced internally with respect to the protio solvent impurity. Deuterated NMR solvents were obtained from Cambridge Isotope Laboratories, Inc., Andover, MA, and used without further purification. Mass spectrometric analysis was performed using a Thermo LTQ linear ion trap with a standard electrospray ionization source

(Thermo Fisher Scientific, San Jose, CA, USA). Samples were directly infused at 3 $\mu\text{L}/\text{min}$ in 100 % MeCN, with the source voltage set to 3 kV, tube lens at 75 kV and the capillary temperature at 270 $^\circ\text{C}$. CID fragment spectra were collected in ZoomScan mode with isolation window = 5 m/z , normalized collision energy (nCE) = 30 and activation time = 30 ms. MS data was analyzed using Thermo XCalibur. Predicted isotope patterns were prepared using ChemCalc. All other materials were obtained from Aldrich Chemical Company, St. Louis, MO, or TCI, Tokyo, Japan and were used as received. Solvents were dried through a commercial solvent purification system (Pure Process Technologies, Inc.). Ligands X ,^{21a} XE ,^{22b} FOH ,⁷ and F ^{22b} were synthesized according to previously published methods. Cage assemblies $\text{Fe}_2\text{X}_3\cdot\text{Py}_6$,^{21a} $\text{Fe}_2\text{XE}_3\cdot\text{Py}_6$,^{22b}, $\text{Fe}_4\text{FOH}_6\cdot\text{Py}_{12}$,⁷ and $\text{Fe}_4\text{F}_6\cdot\text{Py}_{12}$,^{22b} $\text{Fe}_2\text{APA}_3\cdot\text{Py}_6$,²⁰ $\text{Fe}_4\text{APA}_4\cdot\text{Py}_{12}$ ²⁰ and $\text{Fe}_2\text{DPM}_3\cdot\text{Py}_6$ ²⁹ were synthesized according to previously published methods. Minimized geometries were obtained via density functional calculations, optimized using the B3LYP-D3(BJ)/6-31G(d) basis set, and the single point energies calculated with the larger basis set B3LYP-D3(BJ)/def2-TZVP.

Synthesis of New Compounds

4,4'-(9H-xanthene-2,7-diyl)dianiline

(DPX): Di-tert-butyl ((9H-xanthene-2,7-diyl)bis(4,1-phenylene))dicarbamate (see Supporting Information for synthesis) (150 mg, 0.27 mmol) was placed in a 10 mL round bottomed flask with a stir bar. Trifluoroacetic acid (neat, 2 mL) was slowly added to the flask. The reaction mixture was allowed to stir at room temperature for 12 hours. The reaction mixture was then slowly added dropwise to a beaker containing 10 g crushed ice and 30 mL saturated sodium bicarbonate solution. When all the reaction mixture had been added, the pH of the solution was tested, and more bicarbonate solution was added as necessary to reach a pH of 8. The solid product was then filtered, washed with hexane and dried to give DPX as a tan solid (92 mg, 0.252 mmol, 92 %). ^1H NMR (400 MHz, $\text{DMSO}-d_6$) δ 7.43 (d, $J = 2.2$ Hz, 2H), 7.39 (dd, $J = 8.5, 2.3$ Hz, 2H), 7.36 – 7.32 (m, 4H), 7.07 (d, $J = 8.4$ Hz, 2H), 6.66 – 6.62 (m, 4H), 5.18 (s, 4H), 4.13 (s, 2H). ^{13}C NMR (151 MHz, DMSO) δ 150.10 (s), 148.45 (s), 136.26 (s), 127.35 (s), 127.26 (s), 126.30 (s), 125.09 (s), 120.97 (s), 116.70 (s), 114.65 (s), 27.66 (s). (HRMS (ESI+) m/z calcd for $\text{C}_{25}\text{H}_{20}\text{N}_2\text{O}$ 464.21, found 465.1422 ($\text{M}+\text{H}$)⁺.

$\text{Fe}_2\text{DPX}_3\cdot\text{Py}_6$: DPX (50 mg, 0.137 mmol) was added to a 25 mL round bottom and dissolved in acetonitrile (5 mL). 2-pyridinecarboxaldehyde (26.1 μL , 0.274 mmol) was added to the solution followed by $\text{Fe}(\text{OTf})_2$ (38.93 mg, 0.091 mmol), the reaction was heated to 65 $^\circ\text{C}$ for 16 h. The

reaction was cooled to room temperature and diluted with Et₂O. The solution was filtered, and the resulting precipitate was washed with EtOAc to give Fe₂DPX₃•Py₆ as a purple powder (95 mg, 0.041 mmol, 90 %). ¹H NMR and ¹³C NMR: Mixture of two isomers (helicate and mesocate are both present in a 1:2 ratio respectively). ¹H NMR (400 MHz, CD₃CN) δ 9.02 (s, 6H, heli), 8.90 (s, 6H, meso), 8.62 – 8.53 (m, 12H, both), 8.46 – 8.39 (m, 12H, both), 7.84 – 7.76 (m, 12H, both), 7.73 (s, 6H, heli), 7.64 (s, 6H, meso), 7.60 (d, *J* = 8.7 Hz, 6H, meso), 7.54 – 7.51 (m, 12H, both), 7.47 (d, *J* = 5.8 Hz, 6H, meso), 7.45 – 7.40 (m, 24H, both), 7.27 – 7.20 (m, 12H, both), 5.49 (d, *J* = 7.6 Hz, 12H, heli), 5.26 (s, 12H, meso), 4.56 (s, 6H, heli), 4.26 (d, *J* = 18.4 Hz, 3H, meso), 4.16 (d, *J* = 18.4 Hz, 3H, meso). ¹³C NMR (101 MHz, CD₃CN) δ 174.81, 174.56, 158.57, 158.38, 156.20, 153.53, 152.61, 150.02, 149.46, 140.59, 140.00, 135.05, 134.52, 131.63, 131.37, 130.42, 130.10, 128.77, 128.07, 127.74, 127.46, 126.31, 126.01, 125.07, 123.78, 122.65, 122.31, 122.10, 121.89, 117.38, 117.23, 115.52, 28.83, 28.45. HRMS (ESI) *m/z* calcd for C₁₁₂H₇₈F₃Fe₂N₁₂O₆S ([Fe₂(DPX)₃•Py₆(OTf)]³⁺) 629.4852, found 629.48.

General Displacement Conditions. To an NMR tube was added 400 μL of a 7.3 mM solution of mesocate Fe₂X₃•Py₆ in CD₃CN. This solution was checked via ¹H NMR prior to the reaction to confirm the integrity of the sample. To this solution was added 100 μL of the chosen dianiline (87 mM, yielding a final dianiline concentration of 17.4 mM and Fe₂X₃•Py₆ at a concentration of 5.8 mM). The sample was then shaken by hand for ~30 s. A ¹H NMR spectrum was immediately taken following mixing. Periodic monitoring of the sample was then conducted via ¹H NMR to determine the degree and products of the displacement reactions.

FeF₃•Py₃: mesocate Fe₂X₃•Py₆ (20 mg, 0.012 mmol) was added to a 5 mL round bottom flask and dissolved in acetonitrile (1.6 mL). Dianiline **F** (7 mg, 0.036 mmol) was dissolved in 200 μL acetonitrile then added to the cage solution. The solution was shaken for 5 s to facilitate mixing and allowed to sit. After 3 h diethyl ether was added to the solution and the reaction was filtered as a brown powder (7 mg, 0.006 mmol, 54 %). **Fac:** ¹H NMR (400 MHz, CD₃CN) δ 8.87 (s, 3H), 8.47 (d, *J* = 7.6 Hz, 3H), 8.37 (t, *J* = 7.5 Hz, 3H), 7.76 (s, 3H), 7.64 (d, *J* = 7.0 Hz, 1H), 7.24 (d, *J* = 8.6 Hz, 6H), 5.47 (d, *J* = 8.0 Hz, 3H), 5.40 (s, 1H), 3.52 (s, 6H), 3.47 (s, 6H). **Mer:** ¹H NMR (400 MHz, CD₃CN) δ 9.40 (s, 1H), 9.16 (s, 1H), 8.81 (s, 1H), 8.60 (d, *J* = 5.3 Hz, 2H), 8.56 (d, *J* = 8.0 Hz, 2H), 8.50 (d, *J* = 5.4 Hz, 1H), 8.27 (t, *J* = 7.6 Hz, 1H), 7.95 – 7.91 (m, 2H), 7.84 (d, *J* = 8.8 Hz, 2H), 7.76 (d, *J* = 4.8 Hz, 2H), 7.74 – 7.71 (m, 2H), 7.55 (d, *J* = 4.4 Hz, 1H), 7.53 (d, *J* = 6.2 Hz, 2H), 7.51

(d, *J* = 7.7 Hz, 2H), 7.44 (s, 1H), 7.42 (d, *J* = 5.7 Hz, 1H), 7.40 (s, 1H), 7.32 (d, *J* = 8.9 Hz, 2H), 7.19 (d, *J* = 8.1 Hz, 1H), 6.81 (t, *J* = 12.7 Hz, 6H), 6.76 (d, *J* = 13.1 Hz, 3H), 6.70 (dd, *J* = 8.1, 1.9 Hz, 2H), 6.64 (ddd, *J* = 13.8, 8.2, 1.9 Hz, 3H), 6.55 (d, *J* = 8.1 Hz, 1H), 6.30 (d, *J* = 8.1 Hz, 1H), 6.17 (s, 1H), 3.74 (s, 2H), 3.39 (s, 2H) ¹³C NMR (101 MHz, CD₃CN) δ 195.21, 177.09, 173.85, 171.69, 170.12, 159.60, 159.02, 158.80, 157.38, 156.92, 156.23, 149.75, 149.40, 149.24, 148.33, 146.37, 144.76, 144.51, 139.34, 139.11, 138.93, 131.74, 131.14, 130.55, 129.93, 129.44, 128.75, 124.57, 123.78, 122.25, 121.97, 121.80, 121.28, 121.11, 119.80, 119.55, 119.22, 118.81, 117.91, 114.09, 111.23, 111.15, 110.53, 107.65, 36.99, 36.44. HRMS (ESI) *m/z* calcd for C₅₇H₄₅FeN₉ ([Fe(F)₃•Py₃]²⁺) 455.6568, found 455.65. Elemental Analysis: Theoretical (C₅₇H₄₆Cl₃FeN₉O₁₂): C: 56.52, H: 3.83, Cl: 8.78, Fe: 4.61, N: 10.41, O: 15.85. Found: C: 56.25, H: 3.84, N: 9.89.

ASSOCIATED CONTENT

Supporting Information

Characterization and additional spectral data. This material is available free of charge via the Internet at <http://pubs.acs.org>.

AUTHOR INFORMATION

Corresponding Author

* E-mail: richard.hooley@ucr.edu

ACKNOWLEDGMENTS

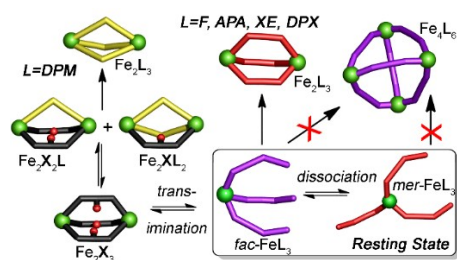
The authors would like to thank the National Science Foundation (CHE-1708019 to R.J.H., CHE-1665212 to G.J.O.B.) and NIH (NIGMS grant R01GM107099 to R.R.J.) for funding, Prof. Hill Harman for structural discussions and Dr. Dan Borchardt for NMR assistance. Supercomputer time from XSEDE (TG-CHE110064, to G.J.O.B.) is also gratefully acknowledged.

REFERENCES

- (1) (a) Ward, M. D.; Raithby, P. R. Functional behaviour from controlled self-assembly: challenges and prospects. *Chem. Soc. Rev.* **2013**, *42*, 1619-1636. (b) Fujita, M.; Tominaga, M.; Hori, A.; Therrien, B. Coordination assemblies from a Pd(II)-cornered square complex. *Acc. Chem. Res.*, **2005**, *38*, 369-380. (c) Cook, T.R.; Stang, P.J. Recent Developments in the Preparation and Chemistry of Metallacycles and Metallacages via Coordination. *Chem. Rev.* **2015**, *115*, 7001-7045.
- (2) (a) Brown, C. J.; Toste, F. D.; Bergman, R. G.; Raymond, K. N. Supramolecular catalysis in metal-ligand cluster hosts. *Chem. Rev.*, **2015**, *115*, 3012-3035. (b) Ueda, Y.; Ito, H.; Fujita, D.; Fujita, M. Permeable Self-Assembled Molecular Containers for Catalytic Isolation Enabling Two-Step Cascade Reactions. *J. Am. Chem. Soc.* **2017**, *139*, 6090-6093. (c) Hastings, C. J.; Pluth, M. D.; Bergman, R. G.; Raymond, K. N. Enzymelike

- Catalysis of the Nazarov Cyclization by Supramolecular Encapsulation. *J. Am. Chem. Soc.* **2010**, *132*, 6938-6940.
- (3) (a) Ronson, T. K.; Giri, C.; Beyeh, N. K.; Minkinen, A.; Topic, F.; Holstein, J.J.; Rissanen, K.; Nitschke, J. R. Size-Selective Encapsulation of Hydrophobic Guests by Self-Assembled M_4L_6 Cobalt and Nickel Cages. *Chem. Eur. J.* **2013**, *19*, 3374-3382. (b) Liu, C.-L.; Zhou, L.-P.; Tripathy, D.; Sun, Q.-F. Self-assembly of stable luminescent lanthanide supramolecular M_4L_6 cages with sensing properties toward nitroaromatics. *Chem. Commun.* **2017**, *53*, 2459-2462.
- (4) (a) Wang, W.; Wang, Y.-X.; Yang, H.-B. Supramolecular transformations within discrete coordination-driven supramolecular architectures. *Chem. Soc. Rev.* **2016**, *45*, 2656-2693. (b) Erbas-Cakmak, S.; Leigh, D. A.; McTernan, C. T.; Nussbaumer, A. L. Artificial Molecular Machines. *Chem. Rev.* **2015**, *115*, 10081-10206. (c) Kay, E. R.; Leigh, D. A. Rise of the Molecular Machines. *Angew. Chem. Int. Ed.* **2015**, *54*, 10080-10088.
- (5) Samanta, S. K.; Moncelet, D.; Briken, V.; Isaacs, L. Metal-Organic Polyhedron Capped with Cucurbit[8]uril Delivers Doxorubicin to Cancer Cells. *J. Am. Chem. Soc.* **2016**, *138*, 14488-14496.
- (6) (a) Caulder, D. L.; Raymond, K. N. Supermolecules by Design. *Acc. Chem. Res.* **1999**, *32*, 975-982. (b) Fujita, M.; Umemoto, K.; Yoshizawa, M.; Fujita, N.; Kusukawa, T.; Biradha, K. Molecular paneling via coordination. *Chem. Commun.* **2001**, 509-518. (c) Young, N. J.; Hay, B. P. Structural design principles for self-assembled coordination polygons and polyhedral. *Chem. Commun.* **2013**, *49*, 1354-1379. (d) Saalfrank, R.W.; Maid, H.; Scheurer, A. Supramolecular coordination chemistry: the synergistic effect of serendipity and rational design. *Angew. Chem. Int. Ed.* **2008**, *47*, 8794-8824.
- (7) Young, M. C.; Holloway, L. R.; Johnson, A. M.; Hooley, R. J. A supramolecular sorting hat: stereocontrol in metal-ligand self-assembly by complementary hydrogen bonding. *Angew. Chem. Int. Ed.* **2014**, *53*, 9832-9836.
- (8) (a) Tsujimoto, Y.; Kojima, T.; Hiraoka, S. Rate-determining step in the self-assembly process of supramolecular coordination capsules. *Chem. Sci.* **2014**, *5*, 4167-4172. (b) Baba, A.; Kojima, T.; Hiraoka, S. Self-Assembly Process of Dodecanuclear Pt(II)-Linked Cyclic Hexagon. *J. Am. Chem. Soc.* **2015**, *137*, 7664-7667. (c) Kai, S.; Sakuma, Y.; Mashiko, T.; Kojima, T.; Tachikawa, M.; Hiraoka, S. The Effect of Solvent and Coordination Environment of Metal Source on the Self-Assembly Pathway of a Pd(II)-Mediated Coordination Capsule. *Inorg. Chem.* **2017**, *56*, 12652-12663.
- (9) Fatin-Rouge, N.; Blanc, S.; Leize, E. Dorselaer, A. V.; Baret, P.; Pierre, J.-L.; Albrecht-Gary, A.-M. Self-Assembly of a Diferrous Triple-Stranded Helicate with Bis(2,2'-Bipyridine) Ligands: Thermodynamic and Kinetic Intermediates. *Inorg. Chem.* **2000**, *39*, 5771-5778.
- (10) (a) Meyer, M.; Kersting, B.; Powers, R.; Raymond, K. N. Rearrangement Reactions in Dinuclear Triple Helicates. *Inorg. Chem.* **1997**, *36*, 5179-5191. (b) Davis, A.V.; Raymond, K. N. The Big Squeeze: Guest Exchange in an M_4L_6 Supramolecular Host. *J. Am. Chem. Soc.* **2005**, *127*, 7912-7919.
- (11) (a) Neogi, S.; Schnakenburg, G.; Lorenz, Y.; Engeser, M.; Schmitt, M. Implications of Stoichiometry-Controlled Structural Changeover Between Heteroleptic Trigonal $[Cu(phenAr_2)(py)]^+$ and Tetragonal $[Cu(phenAr_2)(py)_2]^+$ Motifs for Solution and Solid-State Supramolecular Self-Assembly. *Inorg. Chem.* **2012**, *51*, 10932-10841. (b) Neogi, S.; Lorenz, Y.; Engeser, M.; Samanta, D.; Schmitt, M. Heteroleptic Metallo-supramolecular Racks, Rectangles, and Trigonal Prisms: Stoichiometry-Controlled Reversible Interconversion. *Inorg. Chem.* **2013**, *52*, 6975-6984. (c) Bhat, I. A.; Samanta, D.; Mukherjee, P. S. A Pd_{24} Pregnant Molecular Nanoball: Self-Templated Stellation by Precise Mapping of Coordination sites. *J. Am. Chem. Soc.* **2015**, *137*, 9497-9502. (d) Preston, D.; McNeill, S. M.; Lewis, J. E. M.; Giles, G. I.; Crowley, J. D. Enhanced kinetic stability of $[Pd_2L_4]^{4+}$ cages through ligand substitution. *Dalton Trans.* **2016**, *45*, 8050-8060. (e) Harano, K.; Hiraoka, S.; Shionoya, M. 3 nm-Scale Molecular Switching between Fluorescent Coordination Capsule and Nonfluorescent Cage. *J. Am. Chem. Soc.* **2007**, *129*, 5300-5301. (f) Zhao, L.; Northrop, B. H.; Stang, P. J. Supramolecule-to-Supramolecule Transformations of Coordination-Driven Self-Assembled Polygons. *J. Am. Chem. Soc.* **2008**, *130*, 11886-11888.
- (12) (a) Stadler, A.-M.; Ramirez, J.; Lehn, J.-M.; Vincent, B. Supramolecular reactions of metallo-architectures: Ag_2 -double-helicate/ Zn_4 -grid, Pb_4 -grid/ Zn_4 -grid interconversions, and Ag_2 -double-helicate fusion. *Chem. Sci.* **2016**, *7*, 3689-3693. (b) Funeriu, D. P.; Lehn, J.-M.; Fromm, K. M.; Fenske, D. Multiple Expression of Molecular Information: Enforced Generation of Different Supramolecular Inorganic Architectures by Processing of the Same Ligand Information through Specific Coordination Algorithms. *Chem. Eur. J.* **2000**, 2103-2111.
- (13) Mal, P.; Schultz, D.; Beyeh, K.; Rissanen, K.; Nitschke, J. R. An unlockable-relockable iron cage by subcomponent self-assembly. *Angew. Chem. Int. Ed.* **2008**, *47*, 8297-8301.
- (4) (a) Hristova, Y. R.; Smulders, M. M. J.; Clegg, J. K.; Breiner, B.; Nitschke, J. R. Selective anion binding by a chameleon capsule with a dynamically reconfigurable exterior. *Chem. Sci.* **2011**, *2*, 638-641. (b) Clegg, J. K.; Cremers, J.; Hogben, A.J.; Breiner, B.; Smulders, M. M. J.; Thoburn, J.D.; Nitschke, J. R. A Stimuli Responsive System of Self-assembled Anion-binding $Fe_4L_6^{8+}$ Cages. *Chem. Sci.* **2013**, *4*, 68-76. (c) Bolliger, J. L.; Belenguer, A. M.; Nitschke, J. R. Enantiopure Water-Soluble $[Fe_4L_6]$ Cages: Host-Guest Chemistry and Catalytic Activity. *Angew. Chem., Int. Ed.* **2013**, *52*, 7958-7962.
- (5) (a) Meng, W.; Clegg, J. K.; Thoburn, J. D.; Nitschke, J. R. Controlling the Transmission of Stereochemical Information through Space in Terphenyl-Edged Fe_4L_6 Cages. *J. Am. Chem. Soc.* **2011**, *133*, 13652-13660. (b) Meng, W.; Ronson, T. K.; Nitschke, J. R. Symmetry breaking in self-assembled M_4L_6 cage complexes. *Proc. Natl. Acad. Sci. U.S.A.* **2013**, *110*, 10531-10535.
- (6) (a) Castilla, A. M.; Ronson, T. K.; Nitschke, J. R. Sequence-Dependent Guest Release Triggered by Orthogonal Chemical Signals. *J. Am. Chem. Soc.* **2016**, *138*, 2342-2351. (b) Bilbeisi, R. A.; Ronson, T. K.; Nitschke, J. N. A Self-Assembled $[Fe_{12}L_{12}]$ Capsule with an Icosahedral Framework. *Angew. Chem. Int. Ed.* **2013**, *52*, 9027-9030.
- (7) (a) Wood, D. M.; Meng, W.; Ronson, T. K.; Stefankiewicz, A. R.; Sanders, J. K. M.; Nitschke, J. R. Guest-Induced Transformation of a Porphyrin-Edged Fe_4L_6 Capsule into a $Cu^I/Fe^II_2L_4$ Fullerene Receptor. *Angew. Chem. Int. Ed.* **2015**, *54*, 3988-3992. (b) Meng, W.; Breiner, B.; Rissanen, K.; Thoburn, J. D.; Clegg, J. K.; Nitschke, J. R. A self-assembled M_8L_6 cubic cage that selectively encapsulates large aromatic guests. *Angew. Chem. Int. Ed.* **2011**, *50*, 3479-3483.
- (18) (a) Ciacchia, M.; Di Stefano, S. Mechanisms of imine exchange reactions in organic solvents. *Org.*

- Biomol. Chem.* **2015**, *13*, 646-654. (b) Acharyya, K.; Mukherjee, S.; Mukherjee, P. S. Molecular Marriage through Partner Preferences in Covalent Cage Formation and Cage-to-Cage Transformation. *J. Am. Chem. Soc.* **2013**, *135*, 554-557.
- (19) (a) Zarra, S.; Clegg, J. K.; Nitschke, J. R. Selective Assembly and Disassembly of a Water-Soluble Fe₁₀L₁₅ Prism. *Angew. Chem. Int. Ed.* **2013**, *52*, 4837-4840. (b) Jiménez, A.; Bilbeisi, R. A.; Ronson, T. A.; Zarra, S.; Woodhead, C.; Nitschke, J. R. Selective Encapsulation and Sequential Release of Guests Within a Self-Sorting Mixture of Three Tetrahedral Cages. *Angew. Chem. Int. Ed.* **2014**, *53*, 4556-4560. (c) Mosquera, J.; Ronson, T. K.; Nitschke, J. R. Subcomponent Flexibility Enables Conversion between D₄-Symmetric Cd₈L₈ and T-Symmetric Cd₄L₄ Assemblies. *J. Am. Chem. Soc.* **2016**, *138*, 1812-1815.
- (20) Bilbeisi, R. A.; Clegg, J. K.; Elgrishi, N.; de Hatten, X.; Devillard, M.; Breiner, B.; Mal, P.; Nitschke, J. R. Subcomponent Self-Assembly and Guest-Binding Properties of Face-Capped Fe₄L₄⁸⁺ Capsules. *J. Am. Chem. Soc.* **2012**, *134*, 5110-5119.
- (21) (a) Holloway, L. R.; Young, M. C.; Beran, G. J. O.; Hooley, R. J. High Fidelity Sorting of Remarkably Similar Components via Metal-Mediated Assembly. *Chem. Sci.* **2015**, *6*, 4801-4806. (b) Wiley, C. A.; Holloway, L. R.; Miller, T. F.; Lyon, Y.; Julian, R. R.; Hooley, R. J. Electronic Effects on Narcissistic Self-Sorting in Multicomponent Self-Assembly of Felminopyridine meso-Helicates. *Inorg. Chem.* **2016**, *55*, 9805-9815. (c) Young, M. C.; Johnson, A. M.; Hooley, R. J. Self-Promoted Post-Synthetic Modification of Metal-Ligand M₂L₃ Mesocates. *Chem. Commun.* **2014**, *50*, 1378-1380. (d) Young, M. C.; Johnson, A. M.; Gamboa, A. S.; Hooley, R. J. Achiral Endohedral Functionality Provides Stereochemical Control in Fe(II)-Based Self-Assemblies. *Chem. Commun.* **2013**, *49*, 1627-1629.
- (22) (a) Holloway, L. R.; McGarraugh, H. H.; Young, M. C.; Sontising, W.; Beran, G. J. O.; Hooley, R. J. Structural Switching in Self-Assembled Metal-Ligand Helicate Complexes via Ligand-Centered Reactions. *Chem. Sci.* **2016**, *7*, 4423-4427. (b) Holloway, L. R.; Bogie, P. M.; Lyon, Y.; Julian, R. R.; Hooley, R. J. Stereoselective Postassembly CH Oxidation of Self-Assembled Metal-Ligand Cage Complexes. *Inorg. Chem.* **2017**, *56*, 11435-11442.
- (23) (a) Ronson, T. K.; Pilgrim, B. S.; Nitschke, J. R. Pathway-Dependent Post-assembly Modification of an Anthracene-Edged M₄L₆ Tetrahedron. *J. Am. Chem. Soc.* **2016**, *138*, 10417-10420. (b) Roberts, D. A.; Castilla, A. M.; Ronson, T. K.; Nitschke, J. R. Post-assembly Modification of Kinetically Metastable Fe₂L₃ Triple Helicates. *J. Am. Chem. Soc.* **2014**, *136*, 8201-8204.
- (24) (a) Bloch, W. M.; Abe, Y.; Holstein, J. J.; Wandtke, C. M.; Dittrich, B.; Clever, G. H. *J. Am. Chem. Soc.* Geometric Complementarity in Assembly and Guest Recognition of a Bent Heteroleptic cis-[Pd₂L₂L₂^B]₂ Coordination Cage. **2016**, *138*, 13750-13755. (b) Bloch, W. M.; Holstein, J. J.; Hiller, W.; Clever, G. H. Morphological Control of Heteroleptic cis- and trans-Pd₂L₂L₂ Cages. *Angew. Chem. Int. Ed.* **2017**, *56*, 8285-8289.
- (25) Preston, D.; Bamsley, J. E.; Gordon, K. C.; Crowley, J. D. [Controlled Formation of Heteroleptic \[Pd₂\(L_a\)₂\(L_b\)₂\]⁴⁺ Cages](#). *J. Am. Chem. Soc.* **2016**, *138*, 10578-10585.
- (26) (a) Mal, P.; Nitschke, J. R. Sequential self-assembly of iron structures in water. *Chem. Commun.* **2010**, *46*, 2417-2419. (b) Cu, F.; Li, S.; Jia, C.; Mathieson, J. S.; Cronin, L.; Yang, X.-J.; Wu, B. Anion-Dependent Formation of Helicates versus Mesocates of Triple-Stranded M₂L₃ (M = Fe²⁺, Cu²⁺) Complexes. *Inorg. Chem.* **2012**, *51*, 179-187. (c) Burke, M. J.; Nichol, G. S.; Lusby, P. J. Orthogonal Selection and Fixing of Coordination Self-Assembly Pathways for Robust Metallo-organic Ensemble Construction. *J. Am. Chem. Soc.* **2016**, *138*, 9308-93153. (d) Glasson, C. R. K.; Meehan, G. V.; Motti, C. A.; Clegg, J. K.; Turner, P.; Jensen, P.; Lindoy, L. F. Nickel(II) and iron(II) triple helicates assembled from expanded quaterpyridines incorporating flexible linkages. *Dalton Trans.* **2011**, *40*, 12153-12159.
- (27) Kieffer, M.; Pilgrim, B.S.; Ronson, T.K.; Roberts, D.A.; Aleksanyan, M.J.; Nitschke, J. R. Perfluorinated ligands induce meridional metal stereochemistry to generate M₈L₁₂, M₁₀L₁₅ and M₁₂L₁₈ prisms. *J. Am. Chem. Soc.* **2016**, *138*, 6813-6821.
- (28) (a) Becke, A. D. Density-functional thermochemistry. III. The role of exact exchange. *J. Chem. Phys.* **1993**, *98*, 5648-5652. (b) Rassolov, V. A.; Ratner, M. A.; Pople, J. A.; Redfern, P. C.; Curtiss, L. A. 6-31G* basis set for third-row atoms. *J. Comp. Chem.* **2001**, *22*, 976-984. (c) Weigend, F.; Ahlrichs, R. Balanced basis sets of split valence, triple zeta valence and quadruple zeta valence quality for H to Rn: Design and assessment of accuracy. *Phys. Chem. Chem. Phys.* **2005**, *7*, 3297-3305.
- (29) (a) Hannon, M. J.; Painting, C. L.; Jackson, A.; Hamblin, J.; Errington, W. An inexpensive approach to supramolecular architecture. *Chem. Commun.* **1997**, 1807-1808. (b) Hotze, A. C. G.; Hodges, N. J.; Hayden, R. E.; Sanchez-Can, C.; Paines, C.; Male, N.; Tse, M.-K.; Bunce, C. M.; Chipman, J. K.; Hannon, M. J. Supramolecular Iron Cylinder with Unprecedented DNA Binding Is a Potent Cytostatic and Apoptotic Agent without Exhibiting Genotoxicity. *Chem. Biol.* **2008**, *15*, 1258-1267.



A strained Fe_2L_3 iminopyridine cage shows highly variable reactivity upon post-assembly reaction and allows observation of kinetically trapped intermediates in the self-assembly pathway. The cage allows control of equilibrium processes and direction of product outcomes via small, iterative changes in added subcomponent structure and provides a method of accessing metal-ligand cage structures not normally observed in multicomponent Fe-iminopyridine self-assembly.
